Optimal disturbances above and upstream a flat plate with an elliptic leading edge

By Antonios Monokrousos,[†] Luca Brandt[†1], Catherine Mavriplis[*] and Dan S. Henningson[†]

[†]Linné Flow Centre, SeRC, KTH Mechanics, Stockholm, Sweden
[*]Department of Mechanical Engineering, University of Ottawa, Ottawa, Canada

Technical report, 2011

Adjoint-based iterative methods are employed in order to compute linear optimal disturbances in a spatially growing boundary layer around an elliptic leading edge. The Lagrangian approach is used where an objective function is chosen and constraints are assigned. The optimisation problem is solved using power iterations combined with a matrix-free formulation, where the state is marched forward in time with a standard DNS solver and backward with the adjoint solver until a chosen convergence criterion is fulfilled. We consider the global and the upstream localised optimal initial condition leading to the largest possible energy amplification at time T. We found that the two-dimensional initial condition with the largest potential for growth is a Tolmien-Schlichting-like wave packet that includes the Orr mechanism and is located inside the boundary layer, downstream of the leading edge. Three-dimensional disturbances induce streaks by the lift-up mechanism. Localised optimal initial condition enables us to better study the effects of the leading edge; with this approach we propose a new method to study receptivity. Two-dimensional upstream disturbances, are inefficient at triggering an unstable eigenmode. The three-dimensional disturbances instead induce elongated streamwise streaks; both the global and upstream localised disturbances give significant growth. This advocates for high receptivity to three-dimensional disturbances.

1. Introduction

The flat plate boundary layer has been a test-bed for various approaches when studying hydrodynamic stability. Its relevance arises from the fact that, even if is a fairly simple flow, it contains features of many external flows; thus it is good model for them. In stability studies further simplified versions of the general case are often used with approximations like the locally-parallel assumption with a Fourier decomposition in the streamwise direction (Butler & Farrell 1992; Reddy & Henningson 1993) or slowly varying flow, with parabolized

[1]luca@mech.kth.se

equations (Andersson *et al.* 1999; Luchini 2000; Levin & Henningson 2003; Tempelmann *et al.* 2010)). Two and three-dimensional disturbances have been studied using global modes, and offer an accurate representation of the stability of the growing boundary layer (Åkervik *et al.* 2008). However the effect of the leading edge has not been considered so far.

Recently, with the development of the time-stepper technique, it has become possible to tackle more complicated flow cases with two and three-dimensional disturbances. Essentially stability studies are possible for any type of flow case and/or geometry for which a direct numerical simulation is feasible. The only requirement is a numerical solver of the time-dependent linearised Navier-Stokes equations and the corresponding adjoint problem. This the approach first adopted by Tuckerman & Barkley (2000) and later by Barkley *et al.* (2008), Blackburn *et al.* (2008) and Theofilis (2011) to cite a few names.

This project is an extension to previous work by Monokrousos *et al.* (2010) where optimal disturbances were computed for the case of the flat plate boundary layer. Here we take a step further and include the leading edge of the plate while we still retain a fairly high Reynolds number where typically transitional or even turbulent flow is observed. In particular we focus on the effect of the leading edge, how it can change the optimal disturbances and how the boundary layer can be optimally excited by disturbances coming from the outside.

The flow case, for the chosen parameters is classified as noise amplifier, in contrast to an oscillator. It is characterised by convectively instabilities when studied with the local approach. From the global point of view the flow is asymptotically stable to linear disturbances. Hence it is more relevant to look at the transient growth problem or non-modal analysis.

2. Formulation

The equations to be solved are the linearised Navier-Stokes in the incompressible regime:

$$\begin{aligned} \partial_t \mathbf{u} + (\mathbf{U}\cdot\nabla)\,\mathbf{u} + (\mathbf{u}\cdot\nabla)\,\mathbf{U} &= -\nabla p + Re^{-1}\Delta\mathbf{u} + \mathbf{g}, \\ \nabla\cdot\mathbf{u} &= 0. \end{aligned} \tag{1}$$

The Lagrangian approach is used where an objective function is chosen and constraints are assigned. We are looking for stationary points of the Lagrange functional with respect to the different design variables where optimality is fulfilled. The method is equivalent to finding the leading eigenpair of composite direct and adjoint Navier-Stokes evolution operator. The quantity we choose to maximise, *i.e.* the objective function, is the disturbance kinetic energy at the final time

$$\mathcal{J}(\mathbf{u}) = (\mathbf{u}(T), \mathbf{u}(T)). \tag{2}$$

The chosen constrains are the demand for $\mathbf{u}$ to satisfy the linearised Navies-Stokes and, since we work in the linear framework, we force our initial condition

to unit energy. Hence the Lagrangian functional is written as:

$$\mathcal{L}(\mathbf{u}, \mathbf{u}^*, \gamma) = \mathcal{J} - \int_0^T (\mathbf{u}^*, (\partial_t - \mathcal{A})\,\mathbf{u})\ \mathrm{d}t - \gamma\left((\mathbf{u}(0), \mathbf{u}(0)) - 1\right). \qquad (3)$$

To solve the optimisation problem a matrix-free method is employed, where the state is marched forward in time with a standard direct numerical solver and backward with the corresponding adjoint solver until a chosen convergence criterion is fulfilled.

The problem is initialised with a random field, usually noise. The governing equations are iterated until the action of the combined forward and backward time marching corresponds to pure stretching of the initial condition, i.e. $p_0 = \lambda q_0$, with q_0 being the initial perturbation, p_0 the final field from the adjoint solution and λ a scalar. At convergence q_0 is the optimal disturbance and also an eigenvector of the operator $\mathcal{H}^\dagger\mathcal{H}$ where $\mathcal{H}$ corresponds to the direct operator and $\mathcal{H}^\dagger$ to the adjoint: $\mathcal{H}^\dagger\mathcal{H}q_0 = \lambda q_0$. The action of $\mathcal{H}$ therefore amounts to integrating the linearised Navier-Stokes equations to final time T, where T becomes a parameter of the optimisation.

A similar procedure is applied to find the optimal initial condition localised upstream of the leading edge that undergoes the largest possible amplification as it travels downstream, penetrating the boundary layer. With this approach, we propose a systematic and direct method to compute the receptivity of the boundary layer to external disturbances as the computed optimal modes can be used as a projection basis to quantify the ability of incoming free-stream disturbances to initiate perturbations in the boundary layer. The formulation for localised optimal disturbances was first developed by Monokrousos *et al.* (2010). The optimisation problem is slightly different from the one described above. The new Lagrangian reads

$$\begin{aligned}\mathcal{L}(\mathbf{u}, \mathbf{u}^*, \gamma) = (\mathbf{u}(T), \mathbf{u}(T)) - \int_0^T (\mathbf{u}^*, (\partial_t - \mathcal{A})\,\mathbf{u})\ \mathrm{d}t \\ -\gamma\left((\mathbf{u}(0), \mathbf{u}(0))_\Lambda - 1\right) - (\psi, \nabla\cdot\mathbf{u}(0))_\Lambda \qquad (4)\end{aligned}$$

where the initial condition must exist only inside the sub-domain Λ. Additionally the optimal perturbation must be divergence-free. The inner product defined by $(\cdot,\cdot)_\Lambda$ corresponds to an integral in Λ. For the full derivation we refer to Monokrousos *et al.* (2010).

3. Numerical approach

3.1. *Numerical code*

The governing equations are solved with the spectral element code Nek5000, developed by Tufo & Fischer (2001). The equations are solved by a weighted residual spectral element method (Patera 1984), which allows multi-domain decomposition while preserving high order accuracy. Inside each sub-domain,

refereed to as spectral element, the fields are represented by a spectral decomposition to Legendre polynomials and the grid points follow the Gauss-Lobatto Legendre distribution. For further details see Fischer *et al.* (2008).

The optimisation problem for the optimal initial condition is validated against previous results from Monokrousos *et al.* (2010).

3.2. *Flow case*

We consider a flow around a flat plate with an elliptic leading edge. The leading edge is a modified super-ellipse:

$$\left(\frac{y}{b}\right)^2 = 1 - \left(\frac{a-x}{a}\right)^p \quad \text{where} \quad p = 2 + \left(\frac{x}{a}\right)^2. \tag{5}$$

that has zero curvature at the juncture with the flat section so that no disturbances are introduced by the plate itself. The ratio $\frac{a}{b}$ defines the bluntness and is chosen here $\frac{a}{b} = 6$ which corresponds to a relatively blunt shape, Schrader *et al.* (2010). The Reynolds number of the flow is $Re = \frac{bU}{\nu}$ based on the half thickness of the plate (b), the free-stream velocity (U) and the kinematic viscosity of the fluid (ν). Most of the results presented correspond to Reynolds number $Re = 3000$. We also include few results for a case of lower Reynolds number, $Re = 1000$. In some cases we also provide the Reynolds number based on the distance from the leading edge $Re_x = \frac{xU}{\nu}$ where x is the distance from the leading edge.

In figure 1a) and 1b) the two velocity components of the base flow are shown. Since the flow is globally stable, the base flow is computed marching in time the full non-linear Navier-Stokes equations until a steady state is obtained. The boundary conditions are computed by solving the Euler equations in a domain much larger than our computational domain. A strong deceleration of the flow is observed near the stagnation point, immediately downstream a strong vertical velocity component. Further downstream a thin boundary layer is developing. The computational box extends downstream up to $100 - 200$ units (plate half-with b) depending on the case. For a validation of the base flow see Schrader *et al.* (2010).

3.3. *Resolution*

Since we are using the spectral element method, we decompose our domain in several, relatively large elements. In particular, we used polynomial order 10, which implies 100 points per element for the 2D case and 1000 for the 3D. The total number of elements depends on the length of the box. We run the 2D cases in a longer box (in order to be able to observe an unstable wave packet) using 3040 elements, 19 in the direction normal to the plate and 160 along the plate. The total number of points is 304000. In the 3D cases the computational box was typically shorter and thus we used 124 elements in the streamwise direction. However we needed 3 elements in the spanwise direction to resolve the modulation of the Fourier modes and this gives a total number of

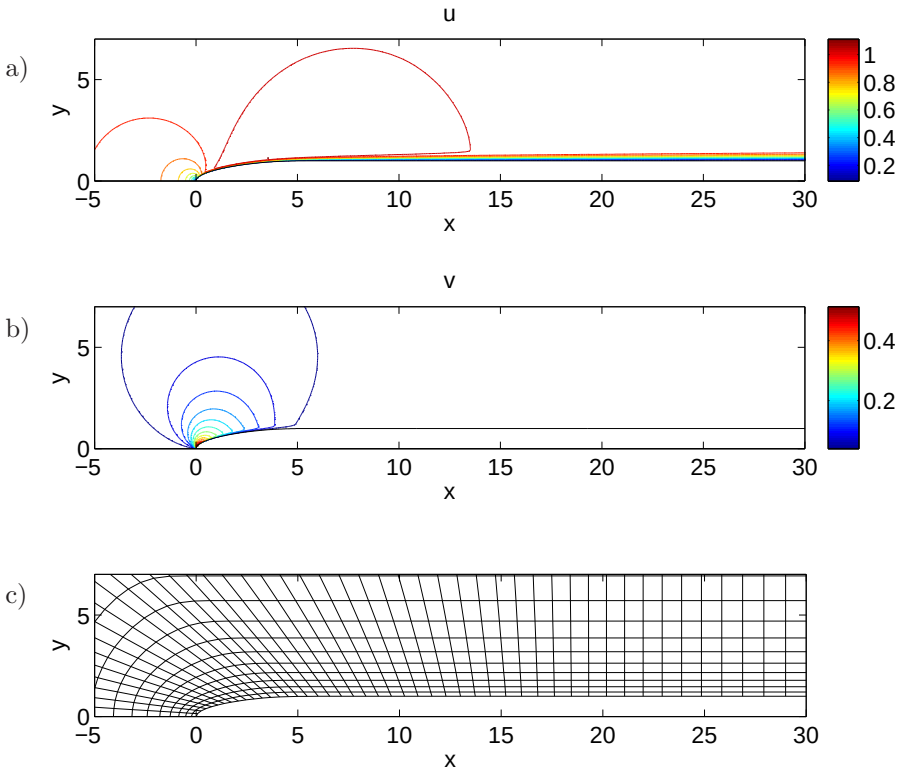

FIGURE 1. Contours of the streamwise (a) and wall-normal (b) velocity components of the base flow for $Re = 3000$. The plot has equal scaling in the two directions. c) Element grid (without the Gauss-Lobatto Legendre points)

elements of 7068. For 3D elements the total number of points is thus 7068000. In both cases we cluster the elements both in the wall-normal direction near the wall and along the plate near the area of the leading edge. A section of the computational grid located around the leading edge is shown in figure 1c).

4. Results

We investigate the disturbances that give the largest transient energy growth. In order to determine the structure in question we loop over different optimisation times. Additionally since the base flow is homogeneous in the spanwise direction, disturbances of different spanwise periodicity are considered separately. Owing to the cost of each optimisation loop, relatively few cases are considered. However, we are confident that the optimal structures are captured and the essential physical mechanisms are included.

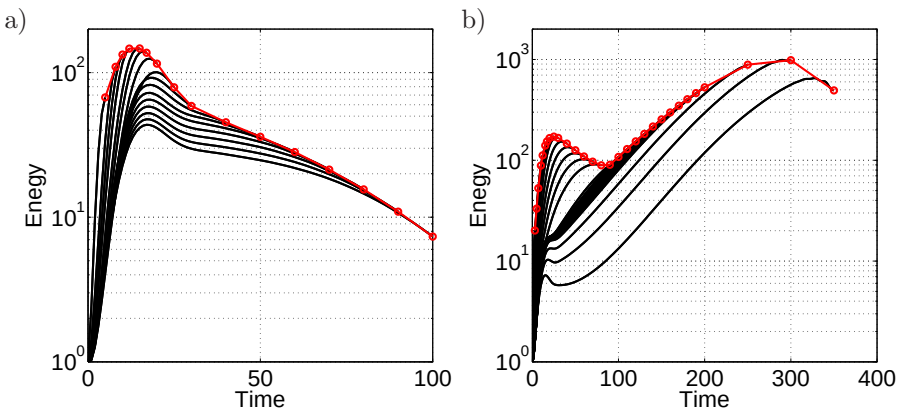

FIGURE 2. Disturbance energy vs optimisation times for $Re = 1000$ (a) and $Re = 3000$ (b) and 2D disturbances.

4.1. *Optimal initial conditions*

First we consider optimal initial condition where no assumptions are made about the location. Two and three dimensional cases are studied.

4.1.1. *Two-dimensional optimal initial conditions*

Two different cases are investigated for the two-dimensional disturbances, one that corresponding to high ($Re = 3000$) and low ($Re = 1000$) Reynolds number.

In figure 2 the disturbance energy growth is shown for the two cases for various optimisation times. The red line is the energy envelope. Figure 2a) shows results for low Reynolds number ($Re = 1000$) where the boundary layer is locally stable all the way down to the outflow. Here the Reynolds number based on the distance to the leading edge is $Re_x = 10^5$. Hence the only way to have energy growth is through the Orr-mechanism. Anything that acts on a longer time scale will only give energy decay.

Figure 2b) reports results for the higher Reynolds number ($Re = 3000$). In this case we observe that locally unstable Tolmien-Schlichting (TS) wave packets are generated and amplify exponentially as they are convected downstream. The maximum time for energy growth is here governed by the downstream extension of the computational box; indeed a longer box would allow longer optimisation times and more space for the exponential instability to grow. Additionally, we note a local maximum for short optimisation times which corresponds again to a pure Orr-mechanism which is active on small time scales. The energy decay seen for large optimisation time is due to the fact that these disturbances gradually exit our computational domain and thus their measurable energy decay.

In figure 3 the spatial structures of the optimal disturbances are shown for the two Reynolds numbers where the optimal times are $T = 12$ ($Re = 1000$) and

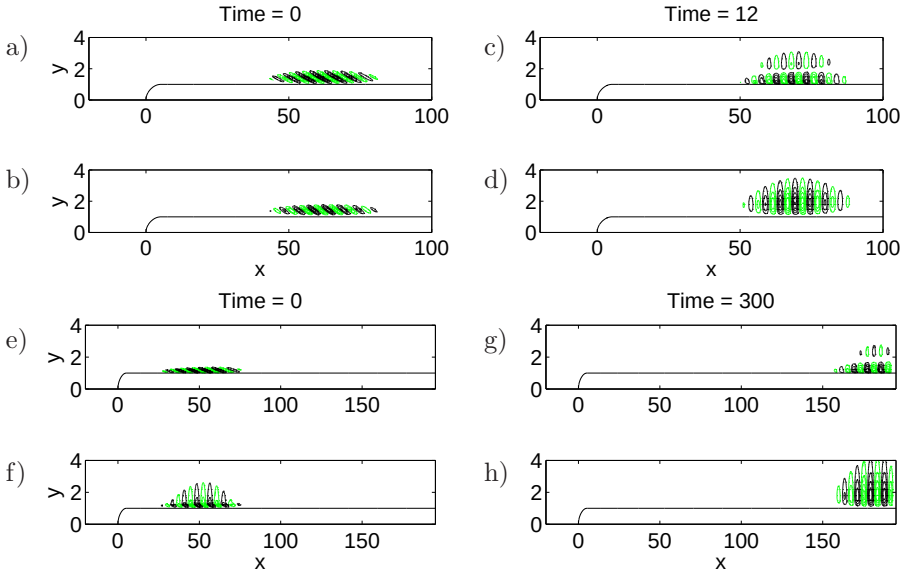

FIGURE 3. Spatial structures for optimal initial condition and the corresponding responses. $Re = 1000$, initial condition: a) streamwise component, b) wall-normal component; response: c) streamwise component, d) wall-normal component. $Re = 3000$, initial condition: e) streamwise component, f) wall-normal component; response: g) streamwise component, h) wall-normal component.

$T = 300$ ($Re = 3000$). The structures look rather similar, Orr-structures generating wave-packets, in both cases (also seen by Monokrousos *et al.* (2010) and Åkervik *et al.* (2008)). However, in the low-Reynolds number case, the energy of the wave-packet decays after the initial increase. Additionally the disturbance is initiated further downstream (relative to the high-Reynolds number case) close to the outflow, exploiting the higher Reynolds number.

4.1.2. *Three-dimensional optimal initial conditions*

Considering three dimensional disturbances, one additional parameter enters the problem, namely the spanwise wavenumber β. To determine the optimal β we need to loop over an additional parameter, as we do for the optimisation time. This leads to a two-dimensional parameter space we need to explore.

In figure (4) we plot iso-contours of energy growth for different optimisation times T and spanwise wavenumbers β. We see a clear peak at $T = 90$ and $\beta = 2.0$. To understand the physical mechanisms behind it we consider the spatial distribution of the disturbance velocities. The three components of the optimal initial condition are shown in figure 5a) and the corresponding response

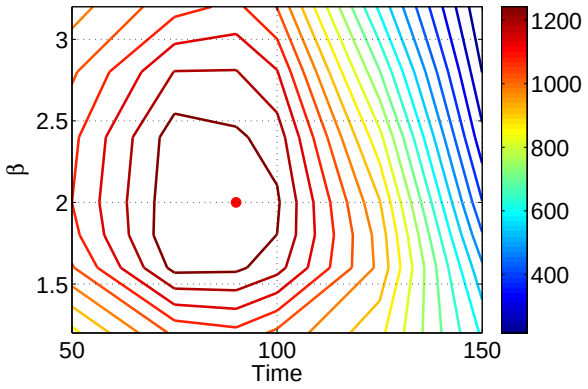

FIGURE 4. Contours of energy gain for different final times and spanwise wavenumbers. The Reynolds number is $Re = 3000$.

	Initial disturbance	Response
Streamwise	6.3 %	91.3%
Wall-normal	28.6%	1.8 %
Spanwise	65.1%	6.9%

TABLE 1. The table shows the component-wise energy content of each component for the initial and final condition. The energy growth was $G = 1.3 \cdot 10^3$

in 5b) while the component-wise energy content is shown in table 1. The time evolution of the three components of the disturbance energy of the perturbation is shown in figure 6.

In table 1 we can see the strong component-wise energy transfer which implies that the lift-up mechanism is active: streamwise vortices induce streamwise streaks inside the boundary layer. Similar results were obtained by Andersson *et al.* (1999) using the boundary layer equations and by Monokrousos *et al.* (2010) in the global framework without the leading edge. The flow structures are plotted in figure 5b). Additionally we can see that the Orr-mechanism with the characteristic upstream leaning structures contribute to some energy gain.

For longer optimisation times a rapid decay of the amplification is observed due to the limited box size, as seen in figure (4). As we increase the optimisation time, the disturbance is forced to move upstream in order to avoid leaving the domain within that time and at some point it goes upstream from the plate, towards the area of the flow where there is not shear. On the other hand for short times, the lift-up mechanism does not have enough time to fully exploit the shear of the boundary layer.

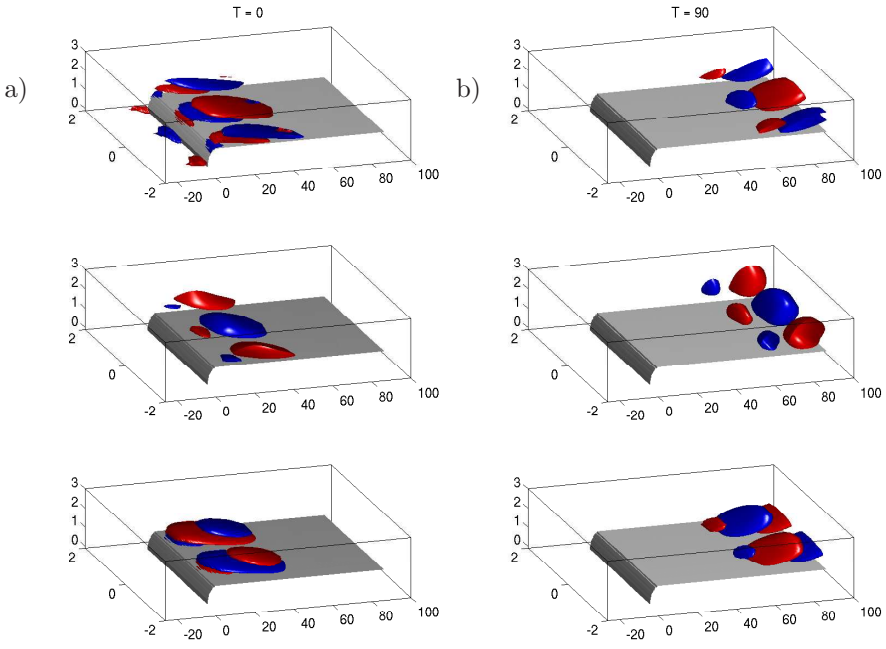

FIGURE 5. Optimal initial condition (a) and the corresponding flow response (b). Streamwise, wall-normal and spanwise velocities are shown from the top to bottom. The energy growth is $G = 1.3 \cdot 10^3$, the Reynolds number, $Re = 3000$. The Reynolds number at the outflow based on the distance from the leading edge is $Re_x = 300000$.

As mentioned above the reported Reynolds number is defined using the free-stream velocity, the half-width of the plate and the fluid viscosity. This implies that all lengths and wavenumbers are scaled with the half-width of the plate. In order to compare with the results from previous studies like Monokrousos *et al.* (2010), where the wavenumber is scaled with the displacement thickness, the length is multiplied with the ratio of the two Reynolds numbers since the free-stream velocity and the viscosity are equal in both cases. In those units the optimal wavenumber is $\beta^* = 0.67$ which is comparable to the value retrieved by Monokrousos *et al.* (2010) ($\beta^* = 0.55$). We should also mention that a variation is to be expected due to the inclusion of the leading edge in the computation.

4.2. *Localised optimal initial conditions*

We study optimal initial conditions that are forced to be localised in space. The used method is extensively described in Monokrousos *et al.* (2010). These

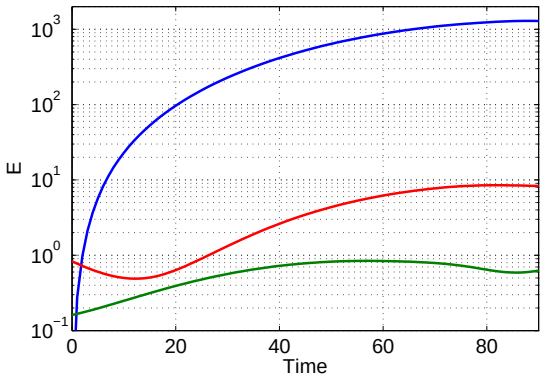

FIGURE 6. Disturbance energy versus time for the optimal initial condition. Three velocity components are shown, streamwise (blue), spanwise (red) and wall-normal (green). The Reynolds number is $Re = 3000$. The Reynolds number as the outflow based on the distance from the leading edge is $Re_x = 300000$.

type of optimals allow us to study how a disturbance optimally penetrates the boundary layer around the curved leading edge and subsequently generates a perturbation that can have a strong growth downstream inside the boundary layer.

4.2.1. *Two-dimensional disturbances*

First we study two-dimensional disturbances. We enforce the initial perturbations to exist in a sub-domain upstream from the leading edge, and thereafter the optimisation procedure gives the optimal spatial distribution inside the sub-domain. In this way we can specifically study the receptivity features. The results we obtained for this case were much in line with Schrader *et al.* (2010). The upstream-localised disturbances are proven to be rather inefficient in penetrating the boundary layer. They loose a lot of energy during the initial phase and furthermore, the disturbance generated inside the boundary layer consists of a wavepacket characterised by a relatively high streamwise wavenumber larger than that corresponding to the unstable TS-wave. Consequently the exponential instability is not efficiently initiated resulting a weak growth in the process.

It appears that the optimisation procedure favours a stable wave-packet over the unstable since it probably has better penetration properties (for this bluntness). In other words, waves of spatial scale of the unstable modes penetrate inefficiently the boundary layer.

To enhance the growth of the wave-packet we would need a much longer computational domain with sufficient space for it to grow exponentially but this would render this computation very expensive.

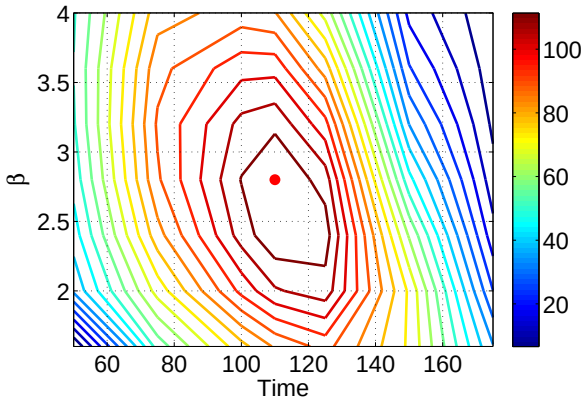

FIGURE 7. Contours of energy gain for different final times and spanwise wavenumbers (localised initial condition). The Reynolds number is $Re = 3000$.

4.2.2. *Three-dimensional disturbances*

As before, we perform a parametric study to find the optimal time and spanwise wavenumber β. In figure (4) iso-contours of energy growth for different optimisation times and spanwise wavenumbers are shown for the case of the upstream localised disturbance. The red dot corresponds to the maximum. The optimal disturbance occurs for $T = 125$ and $\beta = 2.8$. Comparing the values to the non-localised optimal we see two main differences. First the optimisation time is longer and also β is higher. The increased time was expected since the perturbation spends some time upstream from the leading edge and during the penetration phase.

We have seen already that the receptivity to purely two-dimensional disturbances is very weak. That can possibly explain why the optimal β is increased for the upstream localised case, it may become less optimal with respect to the lift-up mechanism but at the same time is less damped by the presence of the leading edge. The two trends seem to balance at $\beta = 2.8$ ($\beta^* = 0.93$).

The physical mechanisms pertaining the energy growth appear to be the same with the exception that the Orr-mechanism is not present. This is attributed to the fact that there is no shear where the perturbation is initiated hence no energy can be gained from an upstream leaning structure.

The spatial distribution of the upstream localised optimal initial condition is shown in figure 8a) and the corresponding response in 8b); in figure 9 we plot the full time evolution of the three components of the energy of the perturbation. We can see that most of the energy of the perturbation lays on the plane normal to the streamwise direction and also the streamwise structure is almost constant implying streamwise vortices that generate streaks inside the boundary layer.

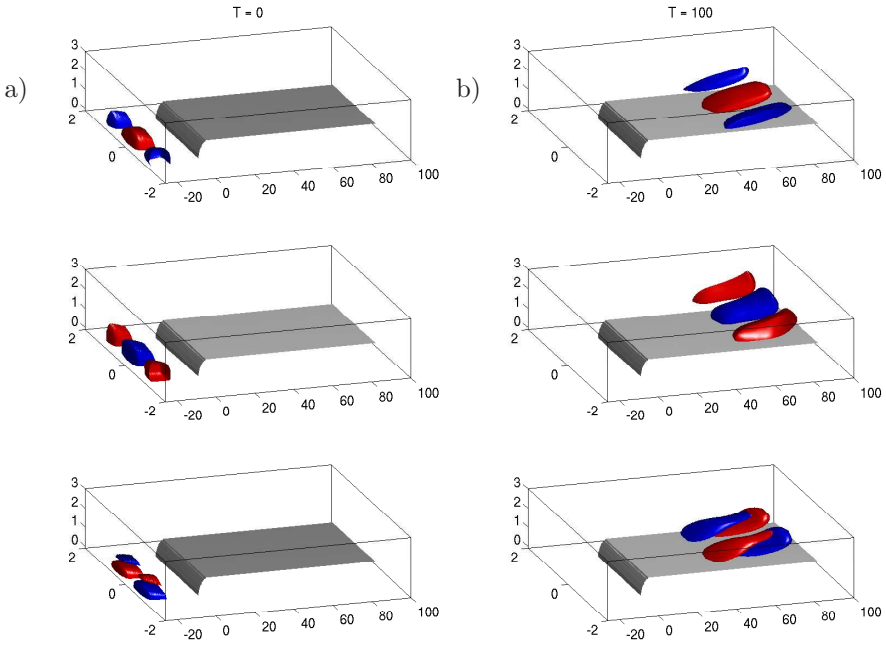

FIGURE 8. Localised optimal initial condition (a) and the corresponding flow response (b). The three components are shown in the vertical order streamwise, wall-normal and spanwise. The energy growth was $G = 1.2 \cdot 10^2$. The Reynolds number is $Re = 3000$. The Reynolds number as the outflow based on the distance from the leading edge is $Re_x = 300000$.

	Initial disturbance	Response
Streamwise	17.7 %	93.6%
Wall-normal	36.7%	1.8 %
Spanwise	45.6%	4.6%

TABLE 2. The table shows the component-wise energy content of each component for the initial and final condition. The energy growth was $G = 1.2 \cdot 10^2$

We note that as the vortices convect downstream in front of the leading edge slowly decay without much happening in the dynamics, similar to what is observed in decaying turbulence. However once they reach the area with strong shear, near the stagnation point ($T \approx 20$), they quickly start to transform energy from the streamwise vortices to the streamwise streaks and through the lift-up effect to extract energy from the mean shear. It is thus important

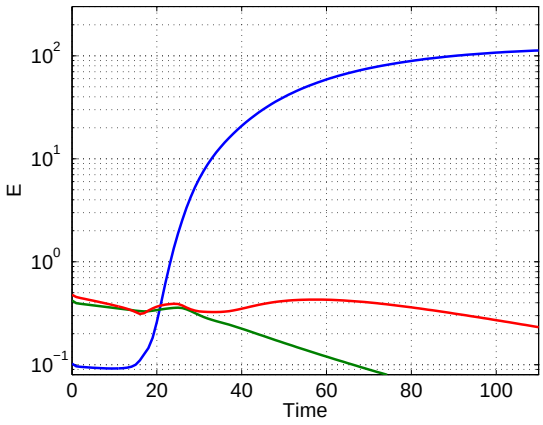

FIGURE 9. Disturbance energy versus time for the optimal localised initial condition. Three velocity components are shown, streamwise (blue), spanwise (red) and wall-normal (green). The Reynolds number is $Re = 3000$. The Reynolds number as the outflow based on the distance from the leading edge is $Re_x = 300000$.

to include the leading-edge effect in receptivity. The total energy growth is substantially weaker relative to the non-localised optimals. This can be attributed to a few reasons. In this case the Orr-mechanisms can not contribute and secondarily the lift-up effect is happening further upstream relative to the non-localised case which corresponds to lower Reynolds number and thus lower transient growth potential, see Andersson *et al.* (1999).

5. Conclusions

We have applied a Lagrange multiplier technique using the direct and adjoint linearised Navier-Stokes equations in order to quantify the disturbance growth potential in a flow around a flat plate with an elliptic leading edge at moderately high Reynolds. We consider the optimal initial condition leading to the largest possible energy amplification at time T. Additionally we compute the localised optimal disturbance upstream from the leading edge. This method can be used to create modal basis and project free-stream disturbances *i.e.* a direct method for computing receptivity coefficients for externally excited flows. The optimisation framework adopted does not restrict us to assume slow variation of the base flow in the streamwise direction, common to both the first order approximation of the Orr-Sommerfeld-Squire formulation and the more advanced Parabolized Stability Equations approximation; moreover, it allows us to include curved geometries and fully three dimensional configurations.

We found that the two-dimensional initial condition with the largest potential for growth is a TS-like wave packet that includes the Orr mechanism in

their initial phase and is located inside the boundary layer, downstream from the leading edge. Its growth is linked to the exponentially unstable eigenmodes of the Blasius boundary layer and it is limited by the streamwise extent of the computational box. The three dimensional case shows a peak in the energy much earlier in time (and space) for spanwise wavenumber $\beta = 2.0$, relevant to the well understood lift-up mechanism. This number is in close agreement with earlier studies of similar nature.

The localised optimal initial conditions are more interesting since they allow for better understanding of the effects of the leading edge and its receptivity properties. Disturbances are placed upstream in the free-stream. We found that the two-dimensional upstream disturbances are rather inefficient at triggering an unstable wave-packet which can exploit the convective instability of the boundary layer. The flow around the leading edge has a strong effect on these type of disturbances, *i.e.* it has a strong damping effect and the later evolution of the disturbance is dominated by this effect. In particular a stable wave-packet is generated and its energy just decays as it propagates downstream inside the boundary layer. This indicates that an unstable wave-packet would be so strongly damped by the leading edge flow that is never favoured by the optimisation.

The three-dimensional disturbances though are exploiting the lift up mechanism very efficiently at a very early stage. The generated streaks are located further from the wall than the TS-wave and thus do not suffer from the loss of energy due to diffusion close to the wall. Additionally their streamwise wavenumber is very low and does not seem to be heavily affected by the low local Reynolds number in the area. This mechanism is proven to be very robust.

6. Acknowledgements

The authors wish to thank Dr. Lars-Uve Schrader for providing the mesh generator and for many fruitful discussions. Computer time provided by SNIC (Swedish National Infrastructure for Computing) is gratefully acknowledged. The present work is supported by the Swedish Research Council (VR) which is gratefully acknowledged.

References

Åkervik, E., Ehrenstein, U., Gallaire, F. & Henningson, D. S. 2008 Global two-dimensional stability measures of the flat plate boundary-layer flow. *Eur. J. Mech. B/Fluids* **27**, 501–513.

Andersson, P., Berggren, M. & Henningson, D. S. 1999 Optimal disturbances and bypass transition in boundary layers. *Phys. Fluids* **11**, 134–150.

Barkley, D., Blackburn, H. M. & Sherwin, S. J. 2008 Direct optimal growth analysis for timesteppers. *Itn. J. Numer. Meth. Fluids* **57**, 1435–1458.

Blackburn, H. M., Barkley, D. & Sherwin, S. J. 2008 Convective instability and transient growth in flow over a backward-facing step. *J. Fluid Mech.* **608**, 271–304.

Butler, K. M. & Farrell, B. F. 1992 Three-dimensional optimal perturbations in viscous shear flow. *Phys. Fluids A* **4**, 1637–1650.

Fischer, P.F., Lottes, J.W. & Kerkemeier, S.G. 2008 nek5000 Web page. Http://nek5000.mcs.anl.gov.

Levin, O. & Henningson, D. S. 2003 Exponential vs algebraic growth and transition prediction in boundary layer flow. *Flow, Turbulence and Combustion* **70**, 183–210.

Luchini, P. 2000 Reynolds-number-independent instability of the boundary layer over a flat surface: Optimal perturbations. *J. Fluid Mech.* **404**, 289–309.

Monokrousos, A., Åkervik, E. & Henningson, L. Brandt D.S. 2010 Global three-dimentional optimal disturbances in the blasius boundary-layer flow using time-steppers. *J. Fluid Mech.* **650**, 181–214.

Patera, Anthony T 1984 A spectral element method for fluid dynamics: Laminar flow in a channel expansion. *Journal of Computational Physics* **54** (3), 468 – 488.

Reddy, S. C. & Henningson, D. S. 1993 Energy growth in viscous channel flows. *J. Fluid Mech.* **252**, 209–238.

Schrader, L.-U., Brandt, L., Mavriplis, C. & Henningson, D. S. 2010 Receptivity to free-stream vorticity of flow past a flat plate with elliptic leading edge. *Journal of Fluid Mechanics* **653** (-1), 245–271.

Tempelmann, D., Hanifi, A. & Henningson, D.S. 2010 Spatial optimal growth in three-dimensional boundary layers. *Journal of Fluid Mechanics* **646**, 5–37.

Theofilis, V. 2011 Global linear instability. *Annual Review of Fluid Mechanics* **43** (1), 319–352.

Tuckerman, L.S & Barkley, D. 2000 *Bifurcation Analysis For Timesteppers*, pp. 453–566. *Numerical Methods for Bifurcation Problems and Large-Scale Dynamical Systems* . Springer, New York.

Tufo, H.M. & Fischer, P.F 2001 Fast parallel direct solvers for coarse grid problems. *Par. & Dist. Computing* **61(2)**, 151–177.